

CFD, Conjugate, Heat, Exchanger, Recuperation

Tytus TULWIN*

MODELLING OF A LARGE ROTARY HEAT EXCHANGER

Abstract

The first simulation consists of a partial cut-out of gas flow canal between the heat exchanger fins. The simulation is steady state and mainly provides the information about the heat transfer coefficient and pressure drop across the canal. The second simulation takes into account the complete system of rotary heat exchanger. It is a transient simulation with moving mesh. Then the heat transfer and air flow parameters are presented as a porous volume with a heat transfer model and rotational multi zone interface conditions. This simplification is accurate providing much better performance as the number of mesh nodes is much smaller. The methodology of the model setup is presented.

1. INTRODUCTION

The industrial rotary heat exchanger is intended to retrieve the heat from the exhaust gases and transfer it to the cold inlet air. This increases the combustion efficiency of the furnace. In order to maximize the heat transfer with minimum pressure drop across the exchanger the CFD simulation method is proposed. The paper presents complete simulation methods for a 5m diameter rotary heat exchanger with 1.4 m disk thickness (Figure 1). The simulation process is split into different parts. Simulating fully represented and detailed honeycomb structure heat transfer would not be feasible because of high number of channels and their complexity. Simplified porous flow and heat transfer method is implemented (Shah & Sekulic, 2003).

* Lublin University of Technology, 38D Nadbystrzycka Str. 20-618 Lublin., +48 81 538 42 50, t.tulwin@pollub.pl

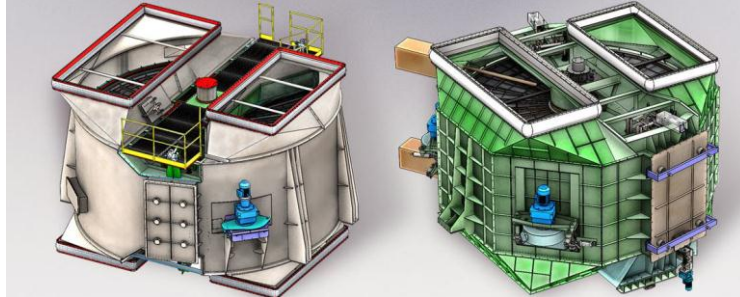


Fig. 1. A large rotary heat exchanger for industrial application (Rotor, 2016)

A large rotary heat exchanger requires a conjugate heat transfer simulation in order to find out its transient characteristics. There are a lot of factors that influence the heat transfer. Some simplifications are made in order to make a robust simulation. The results show how the rotary heat exchanger heats up in time. The heat transfer and air flow conditions are presented for different types of heat exchanger fins. Calculations of temperature data approximation with an aid of lumped heat transfer model are presented. The resultant turbulence conditions are presented showing the relationship between the heat transfer and flow conditions.

2. MATERIALS AND METHODS

2.1. Partial channel model

The circular honeycomb matrix of the rotary heat exchanger consists of two parts: hot end and cold end (Fig. 2). The hot end is made of corrugated steel elements in cross pattern. This type of channels is proven to have a good heat transfer characteristics compared to the pressure drop. It forces some mixing of gas throughout the channels. The thickness of corrugated steel plates is 0.7 mm. The cold end plates are set in a parallel pattern as they are prone to the atmospheric effects like condensation and corrosion. The channels are represented by small section cutouts split in symmetry and periodic planes. Those regions are later treated by respective boundary conditions (Ciofalo, Stasiek & Collins, 1996).

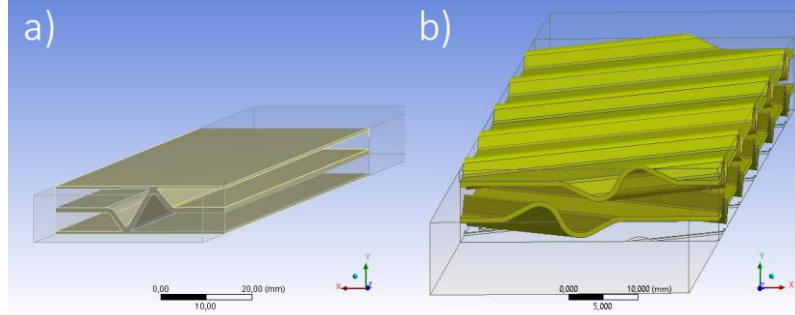


Fig. 2. Hot end channels and cold end channels respectively; single channels section cut-outs as the computational domain

Table 1 presents geometrical information about hot and cold end channels. Porosity and interfacial area density are needed in porous model simulations. Interfacial area density is the ratio of the area of the fluid/solid (“Ansys”, 2016).

Tab. 1. Geometrical properties of the heat exchanger channels

Property		Hot end	Cold end
Overall channel surface area	m ²	8.07E-02	6.3248E-02
Overall channel volume	m ³	1.92E-04	1.5244E-04
Frontal channel surface area	m ²	3.84E-04	3.8110E-04
Frontal solid surface area	m ²	5.68E-05	9.0440E-05
Channel length	m	0.5	0.4
Channel width	m	0.037247	0.0370
Channel height	m	0.0103	0.0103
Porosity	–	0.851975811	0.762687
Interfacialareadensity	m ⁻¹	4.21E+02	4.15E+02

The CFD simulation requires domain discretization into small elements. The computational mesh for the hot end channel consists of mostly tetragonal mesh between the passages and hexagonal in inlet and outlet volumes (Fig. 3a). The cold end mesh consists of hexahedral swept mesh (Fig. 3b). The side walls are represented by linear periodic boundary condition. For both cases, top and bottom walls are symmetry boundary conditions. The hot end grid has 1’517’021 nodes and 3’431’863 elements. The cold end grid has 720’225 nodes and 850’040 elements.

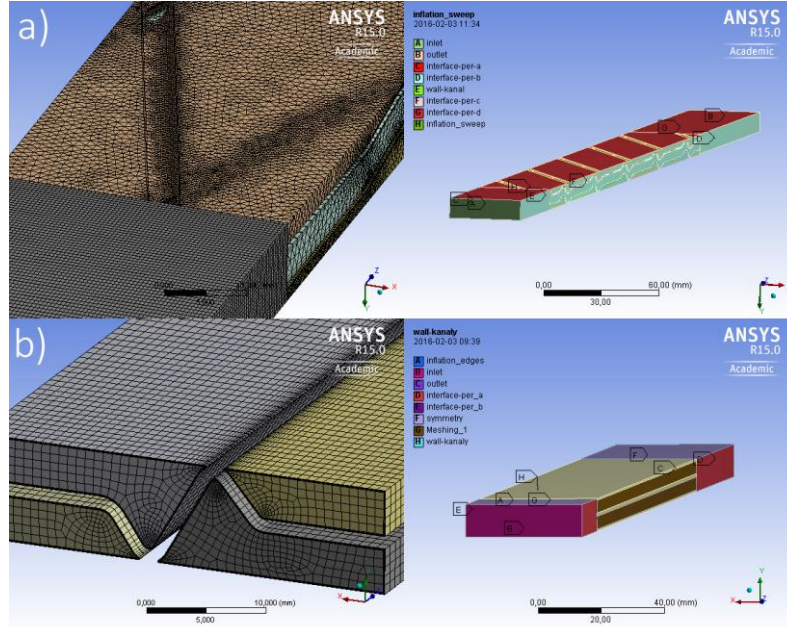


Fig. 3. The computational mesh for the hot partial channel domain

The simulation for both cases is steady state with viscous and compressible fluid. The heat capacity is set as constant. The viscosity and conductivity is represented by the linear function according to the values in table 2.

Tab. 2. Gas properties for different temperatures: conductivity and viscosity

T [K]	k [W/mk]	u [kg/ms]
300	0.02624	1.846e-05
600	0.04661	3.017e-05

Similar method was proposed in the paper (Alekseev, Kostukov, Makarov & Merzlikin, 2016).

2.2. Porous stack model

The resultant pressure drop and heat transfer coefficient from previous partial simulations are the input conditions for the simplified simulation if porous stack model. The simplification is made in means of replacing numerous and dense channels by the porous model. With proper input parameters, the pressure drop characteristics should be matching the results of the partial channel simulation.

The heat transferred model is considered as well by the non-equilibrium thermal model equations. In this case a dual cell approach is used. A solid zone domain is coincident with the fluid zone domain. The only interaction between the zones is the heat transfer solved by conservation equations. The source terms are represented by the equation 1. The transient conduction in the solid region is represented as well as the heat capacity of the solid material. The turbulence is modeled as there would be no effect of solid medium. In this case, such simplification is justified as the main region of interest is the heat transfer. The turbulence effect is included in the heat transfer coefficient calculated in the previous partial models. The porous model together with non-equilibrium thermal model and source terms allow for transient heat transfer considerations (“Ansys”, 2016).

3. RESULTS

3.1. Channel flow characteristics

For each channel 30 different cases of gas temperature and flow velocity were analysed. The parameters that are transferred to the next porous stack simulation are heat transfer coefficient and pressure drop. The heat transfer coefficient’s reference temperature is the average gas temperature in the channel. The heat transfer coefficient is calculated from the basic convection equation. The boundary condition for solid contact is the heat flux density. It is set as constant value of 160 W/m² for the experiment so that the htc can be calculated in every part of the model.

$$Q = A \cdot h (T_{\infty} - T) \quad (1)$$

where: Q – heat flux (W), A – heat transfer area (m²), T_{∞} – reference temperature, T – average solid surface temperature.

Figure 4 shows the results of pressure drop across channels.

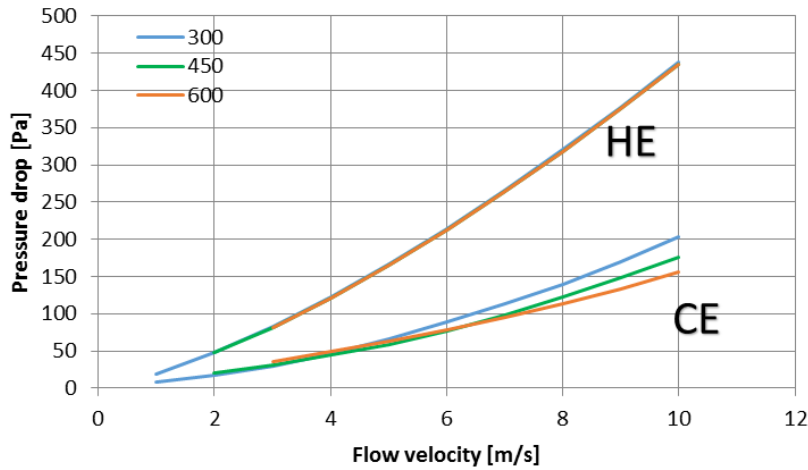


Fig. 4. Pressure vs velocity for hot end and cold end channels for 3 different temperatures

The pressure rise in respect to inlet velocity can be closely represented by the 2nd order polynomial for each case. For hot end channels the pressure drop doesn't change much with temperature change in range of 300–600K ($\ll 1\%$ change). For cold end channels the pressure drop changes with temperature. The increase of temperature decreases the flow resistance. The hot end channels produce much higher pressure drop than the cold end channels. Table 3 and 4 show derived coefficients of viscous resistance C2 and 1/a for cold and hot end, based on velocity and pressure data.

$$y = X1 \cdot x + X2 \cdot x^2 \quad (2)$$

They are calculated with the formula 2 based on X1 and X2 values being 2nd degree polynomial curve fit constants. The parameters: Δm – porous media thickness, ρ – gas density and μ – viscosity.

Tab. 3. Parameters for channel flow resistance calculations – hot end (own study)

X2	ρ	Δm	C2
2.2354	1.147664	0.5	7.791130505
X1	μ	Δm	1/a
20.544	1.78E-05	0.5	2.31E+06

Tab. 4. Parameters for channel flow resistance calculations – cold end (own study)

X2	ρ	Δm	C2
1.4304	1.16085	0.4	6.161
X1	μ	Δm	1/a
5.7929	1.78E-05	0.4	8.14E+05

The porous resistance is calculated based on combination of Darcy’s law and internal loss source term (formula 3) (“Ansys”, 2016; Whitaker, 1985).

$$\Delta p = - \left(\frac{\mu}{\alpha} v + C_2 \frac{1}{2} \rho v^2 \right) \Delta m \quad (3)$$

Figure 5 presents the heat transfer coefficient in respect to flow velocity for the hot and cold end channels. Three different flow temperatures were analysed. The heat transfer coefficient for the hot end channels can be represented by the 2nd order polynomial function for the whole range of temperatures.

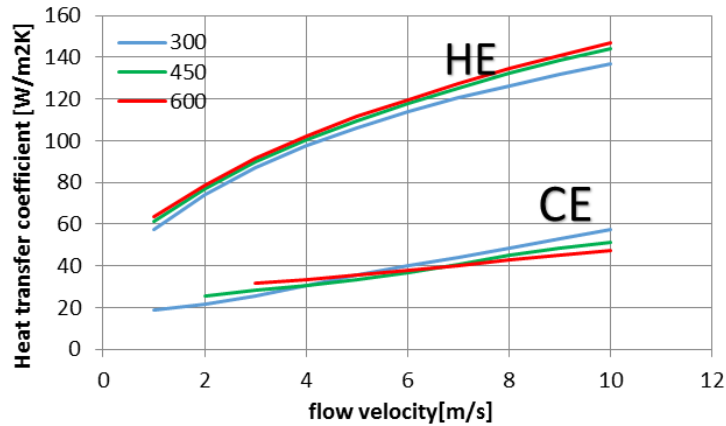


Fig. 5. The heat transfer coefficient in respect to flow velocity for 3 different temperatures

The higher the temperature the higher the heat transfer coefficient for each flow velocity ranging from 1–10 m/s. For the cold end channels the htc function can be represented by the linear function for velocity range of 1–10 m/s and 3 different temperatures 300, 450 and 600 K respectively. Below around 5 m/s the increase of temperature result in increase of the htc. Above 5 m/s this relation is opposite. The heat transfer coefficient is higher for the hot end channels than for the cold end channels. Generally increasing the porosity of channels increases the heat transfer effectiveness (Mahesh, Jayaraman & Madhumitha, 2016).

The effectiveness can reach values as high as 50%. The leakage between zones can vary from 4 to 50% (Alonso, Lui, Mathisen, Ge & Simonson, 2015). Latent heat recovery is also possible using the thermal wheel with an aid of special condensation coating (Nasr, Fauchoux, Besant & Simonson, 2013).

3.2. Transient stack heating

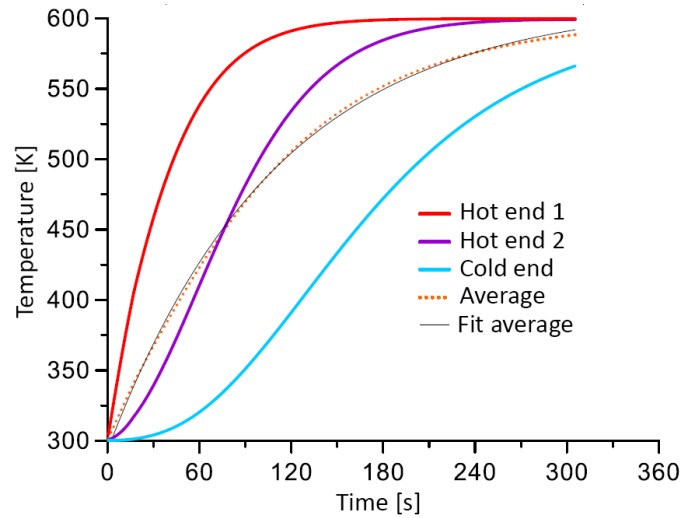


Fig. 6. The heat exchanger disk matrix average temperatures for different layers in respect to simulation time

Figure 6 shows the change of temperature in respect to simulation time for 3 different layers of the heat exchanger disk. First two layers consist of the hot end channels being 500 mm thick. 3rd layer is 400mm thick and consist of the cold end channels. The first hot end channel layer heats up first and reaches the gas temperature after around 180s. The second hot end layer heats up after around 250s. The 3rd cold end layer takes more than 400 s to reach the gas temperature.

The average disk temperature can be approximated by the power-law function:

$$y(x) = A \cdot B^x + C$$

The curve fit constants can be used in the lumped heat transfer model as the Biot-number doesn't exceed the value of 0.1 (Campo, 2012; Cengel & Ghajar, 2014). It must be noted that increasing the rotational speed of rotor can decrease the efficiency of the heat transfer (Grzebielec, Rusowicz & Rucinski, 2014).

4. CONCLUSION

The hot end type channels are more efficient in means of the heat transfer and pressure drop by approximately 25% to 10% with the flow velocity ranging from 1 to 10 m/s respectively. The reason why cold end channels are used is the corrosive nature of the inlet gases. The low temperature of the flowing gas can cause water condensation and excessive corrosion and erosion. The turbulence only amplifies these effects so channels are made to cause as little disturbance to the flow as possible gently heating preheating the air. The cold end channels usually have special coating to prevent corrosion. The proposed porous model can describe the transient heat transfer well (Fig. 6). The temperature data can be used to find out the transient constant in the lumped system model formula.

REFERENCES

- Alekseev, R. A., Kostukov, A. V., Makarov, A. R., & Merzlikin V. G. (2016). Simulation of Characteristics of Thermo-Hydraulic Process in Porous-Net Matrix of Rotary Heat Exchanger. *Global Journal of Pure and Applied Mathematics*, 12(4), 2829–2838.
- Alonso, M. J., Lui, P., Mathisen, H. M., Ge, G., & Simonson, C. (2015). Review of heat/energy recovery exchangers for use in ZEBs in cold climate countries. *Building and Environment*, 84, 228-237. doi:10.1016/j.buildenv.2014.11.014
- Ansys. (n.d.). Program documentation.
- Campo, A. (2012). A new 1-D composite lumped model facilitates the algebraic calculation of local temperatures, mean temperatures, and total heat transfer in simple bodies. *Heat Mass Transfer*, 48(9), 1495–1504. doi:10.1007/s00231-012-0994-x
- Cengel, Y. A., & Ghajar, A. J. (2014). *Heat and Mass Transfer: Fundamentals & Applications* (5 ed.). McGraw-Hill.
- Ciofalo, M., Stasiek, J., & Collins, M. W. (1996). Investigation of flow and heat transfer in corrugated passages—II. Numerical simulations. *International Journal of Heat and Mass Transfer*, 39(1), 165–192. doi:10.1016/S0017-9310(96)85014-9
- Grzebielec, A., Rusowicz, A., & Rucinski, A. (2014). Analysis of the performance of the rotary heat exchanger in the real ventilation systems. *The 9th International Conference. Environmental Engineering, VGTU, Vilno*. doi:10.3846/enviro.2014.259
- Mahesh, S., Jayaraman, B., & Madhumitha, R. (2017). Analysis of Air-to-Air Rotary Regenerator for HVAC Systems Using CFD. In Bajpai R., & Chandrasekhar U. (Eds.) *Innovative Design and Development Practices in Aerospace and Automotive Engineering. Lecture Notes in Mechanical Engineering*. (pp. 455–462). Springer. doi:10.1007/978-981-10-1771-1_49
- Nasr, M. R., Fauchoux, M., Besant, R. W., & Simonson C. J. (2013). A review of frosting in air-to-air energy exchangers. *Renewable and Sustainable Energy Reviews*, 30, 538–554. doi:10.1016/j.rser.2013.10.038
- Rotor. (n.d.). Retrieved November 1, 2016, from Rotor website, <http://www.rotor.lublin.pl>
- Shah, R. K., & Sekulic, D. P. (2003). *Fundamentals of Heat Exchanger Design*. John Wiley & Sons.
- Whitaker, S. (1985). Flow in porous media I: A theoretical derivation of Darcy's law. *Transport Porous Media*, 1(1), 3-25. doi:10.1007/BF01036523